Identification of Linear Systems in the Presence of Nonlinear Distortions

Rik Pintelon, *Fellow, IEEE*, Johan Schoukens, *Fellow, IEEE*, Wendy Van Moer, *Student Member, IEEE*, and Yves Rolain, *Senior Member, IEEE*

***Abstract*—This paper treats the identification of linear systems in the presence of nonlinear distortions. It extends the theory developed in [1] for measurement setups where the input is exactly known and the output is observed with errors (output error framework) to measurement setups where both the input and output are observed with errors (errors-in-variables framework). An appropriate measurement strategy and identification algorithm are presented.**

***Index Terms*—Frequency domain, linear systems, nonlinear distortions, nonparametric noise models, system identification.**

I. Introduction

In LINEAR system identification, a complex (distributed and/or nonlinear) process is approximated by a linear (lumped) dynamic model. The validity (utility) of the linear model is application dependent and should be established in practice. While the influence of random (measurement) errors on the identified linear models is well understood [2], [3], the effect of nonlinear distortions has only recently been studied [1], [4]–[6]. Most of the effort has been spent to analyze the impact (detection, qualification, and quantification) of nonlinear distortions on frequency response function (nonparametric transfer function model) measurements [1], [4]–[6]. The identification of parametric transfer function models in the presence of nonlinear distortions has been treated in [1] for measurement setups where the input is exactly known and the output is observed with errors (output error framework). The contributions of this paper are i) generalization of the results of [1] to measurement setups where both the input and output are corrupted by errors (error-in-variables framework), and ii) development of an improved identification algorithm for the best linear approximation of a nonlinear system.

The class of nonlinear distortions considered in this paper is restricted to those nonlinear systems which can be approximated arbitrarily well in a least squares sense by a Volterra series on a given input domain [7]. This class allows describing strongly nonlinear phenomena like saturation (e.g., amplifiers) and discontinuities (e.g., relays, quantizers). This is not in contradiction with the well-known fact that a Volterra series is only suitable for describing weakly nonlinear systems. Indeed, in a classical Volterra series expansion, the approximation error (difference between the true output and output of the Volterra series) converges everywhere to zero at the same rate as the number of terms in the series tends to infinity (= uniform convergence), while here it is only required that the power of the approximation error tends to zero (= pointwise convergence). The pointwise convergence (approximation in least squares sense) does not exclude that the approximation error remains large at a discrete set of isolated points (similar to a Fourier series approximation of a discontinuous function), which is not the case for the uniform convergence. Nonlinear phenomena for which the theory does not apply are bifurcations, chaos, and subharmonics.

The goal of a linear identification experiment in the presence of nonlinear distortions can be the identification of the true underlying linear system or the best linear approximation of the overall system including the nonlinearities. The first case is useful for physical modeling and, if the system behaves linearly for small inputs, then crest-factor-optimized excitation signals are most suited for the identification experiment [3], [6]. The second case is useful if a linear input/output description is required for a certain class of excitation signals. This paper handles the second case.

The paper is organized as follows. Section II studies the response of a nonlinear system to the class of random-phase multisine excitations. Section III presents an appropriate measurement strategy and identification algorithm for the best linear approximation (also called related linear dynamic system) of the overall system. The theory is illustrated by a simulation (Section IV) and a real measurement example (Section V).

II. Study of the Influence of the Nonlinear Distortions

A. Class of Excitation Signals

The response of the nonlinear system is studied for random-phase multisine excitations. This is a periodic signal with a deterministic user-defined amplitude spectrum and a random-phase spectrum. Following the lines of [1], the results presented in this section can easily be generalized to periodic Gaussian noise (Rayleigh distributed amplitude and uniformly distributed phase spectrum) and to Gaussian noise excitations.

Definition 1: A signal $u(t)$ is a normalized random-phase multisine excitation if

$$\begin{aligned} u(t) &= N^{-1/2} \sum_{k=-N}^{N} A(kf_s/N) e^{j2\pi k f_s t/N} \\ &= N^{-1/2} \sum_{k=1}^{N} 2|A(kf_s/N)| \\ &\quad \cdot \cos(2\pi k f_s t/N + \angle A(kf_s/N)) \end{aligned} \tag{1}$$

Manuscript received May 4, 2000; revised April 17, 2001. This work was supported by the Fund for Scientific Research (FWO-Vlaanderen), the Flemish Government (GOA-IMMI), and the Belgian Program on Interuniversity Poles of Attraction initiated by the Belgian State, Prime Minister's Office, Science Policy programming (IUAP 4/2).

The authors are with the Electrical Measurement Department, Vrije Universiteit Brussel, Brussels, Belgium (e-mail: Rik.Pintelon@vub.ac.be).

Publisher Item Identifier S 0018-9456(01)06011-9.

with $A(-f) = \overline{A}(f)$ ($\overline{\ }$ denotes the complex conjugate) and $0 \leq |A(f)| \leq C < \infty$. $|A(f)|$ has a countable number of discontinuities in the band $[0, f_{\max}]$ with $0 < f_{\max} < f_s/2$, and $A(f) = 0$ for $f = 0$ and $f > f_{\max}$. $\angle A(f)$ is the realization of an independent uniformly distributed random process on $[0, 2\pi)$. The frequencies $f_{\max}$ and f_s are independent of N. □

Note that the random-phase multisine (1) contains $F = Nf_{\max}/fs$ sinewaves.

B. Class of the Nonlinear Systems

We assume that the output of the nonlinear system can be approximated arbitrarily well in least squares sense by a Volterra series on a given input domain. Consider now the steady state response $y(t)$ of such a system to a random-phase multisine $u(t)$ (1), and define $U(k)$ and $Y(k)$ as the scaled DFT spectra of, respectively, N samples of the excitation $u(t)$ and the response $y(t)$

$$X(k) = N^{-1/2} \sum_{n=0}^{N-1} x(nT_s) e^{-j2\pi kn/N} \tag{2}$$

with $X = U$, Y, $x = u$, y, and T_s the sampling period. $U(k)$ and $Y(k)$ are related by

$$Y(k) = \sum_{n=1}^{\infty} Y^n(k) \tag{3}$$

where $Y^n(k)$ stands for the nonlinear contribution of degree n

$$Y^n(k) = N^{-n/2} \sum_{k_1, k_2, \ldots, k_{n-1} = -N}^{N} G^n(s_{k_1}, s_{k_2}, \ldots, s_{k_n}) \cdot U(k_1)U(k_2)\cdots U(k_n) \tag{4}$$

with $k = \sum_{i=1}^{n} k_i$, $G^n(s_{k_1}, s_{k_2}, \ldots, s_{k_n})$ the symmetrized frequency domain representation of the Volterra kernel of degree n [7], [8], and $U(k) = A(kf_s/N)$. Note that the symmetrized kernel is independent of the order of its arguments.

C. Related Linear Dynamic System

For random-phase multisines (see Definition 1), we can distinguish between deterministic and zero mean stochastic contributions in (3). Note that stochastic in this context means stochastic w.r.t. the different realizations of the random phases $\angle A(kf_s/N)$ of the excitation $u(t)$. In [1], it has been shown that (3) can be written as

$$Y(k) = (G_0(s_k) + G_B(s_k))U(k) + Y_S(k) \tag{5}$$

with $G_0(s_k) = G^1(s_k)$ the transfer function of the true underlying linear system. $G_B(s_k)$ is the bias or deterministic nonlinear contribution in (3)

$$G_B(s_k) = \sum_{n=2}^{\infty} G_B^{2n-1}(s_k) \tag{6}$$

where

$$G_B^{2n-1}(s_k) = \frac{c_n}{N^{n-1}} \sum_{k_1, \ldots, k_{n-1}=1}^{N} G^{2n-1} \cdot \left(-s_{k_1}, s_{k_1}, \ldots, -s_{k_{n-1}}, s_{k_{n-1}} s_k\right) \cdot |U(k_1)|^2 \cdots |U(k_{n-1})|^2$$

with $c_n = 2^{n-1}(2n-1)!!$, and $Y_S(k)$ is the zero mean stochastic nonlinear contribution in (3), which is uncorrelated with the input spectrum

$$E\left\{Y_S(k)\overline{U}(k)\right\} = E\{Y_S(k)\}E\left\{\overline{U}(k)\right\} = 0. \tag{7}$$

The sum

$$G_R(s_k) = G_0(s_k) + G_B(s_k) \tag{8}$$

is called the related linear dynamic system. It clearly depends on the amplitude spectrum of the random-phase multisine, and is independent of the even degree nonlinear distortions.

Multiplying (5) by the complex conjugate $\overline{U}(k)$ of the input DFT spectrum, and taking the expected value, gives, using (7)

$$G_R(s_k) = \frac{E\left\{Y(k)\overline{U}(k)\right\}}{E\left\{|U(k)|^2\right\}}. \tag{9}$$

Equation (9) shows that within the class of random-phase multisines with a given amplitude spectrum it makes sense to describe the input/output behavior of the overall system, including the nonlinearities, by the related linear dynamic system $G_R(s_k)$. Similar results are valid for periodic Gaussian noise and asymptotically ($N \to \infty$) valid for Gaussian noise if the expected values in (9) are also taken w.r.t. to the random amplitudes of the excitation $u(t)$ (see [1]). The related dynamic system then becomes

$$G_R(s_k) = G_0(s_k) + E\{G_B(s_k)\} \tag{10}$$

where the expected value is taken w.r.t. the random amplitudes in (6). It can be shown that the related dynamic system (10) of the (periodic) Gaussian noise is related to that (6) of the random-phase multisine by

$$\lim_{N\to\infty} E\{G_B(s_k)\} = \lim_{N\to\infty} G_B(s_k). \tag{11}$$

Since (9) is nothing else than the division of the cross-power by the auto-power spectrum, the related dynamic system is also the best linear approximation in a least squares sense. The advantage of using random-phase multisines over (periodic) Gaussian noise to measure $G_R(s_k)$ is that additional averages over the random amplitudes are avoided. The advantage of using periodic Gaussian noise over Gaussian noise to measure $G_R(s_k)$ is that the leakage errors are avoided. For random-phase multisines, $|U(k)|^2$ is deterministic and (9) can be simplified to

$$G_R(s_k) = E\{Y(k)/U(k)\}. \tag{12}$$

D. Properties of the Stochastic Nonlinear Contributions

Multiplying (5) by $e^{-j\angle U(k)}$ gives

$$Y(k)e^{-j\angle U(k)} = G_R(s_k)|U(k)| + Y_S(k)e^{-j\angle U(k)}. \quad (13)$$

Written in this form, it is obvious that $Y_S(k)e^{-j\angle U(k)}$ is independent of the signal term $G_R(s_k)|U(k)|$. The stochastic behavior of $Y_S(k)e^{-j\angle U(k)}$ has been studied in [1]. It turns out that it has similar properties as the measurement noise; for example, it has zero mean, is asymptotically $(N \to \infty)$ uncorrelated over the frequency k, and is uncorrelated with the input signal. This analysis motivates the block diagram of Fig. 1.

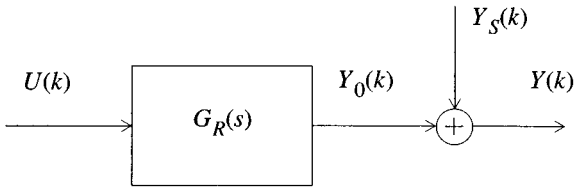

Fig. 1. Input/output behavior of a nonlinear system excited by a random-phase multisine.

III. Identification in the Presence of Nonlinear Distortions

A. Noise and the System Model

In most identification experiments, both the input $u(t)$ and output $y(t)$ are observed and hence are subject to measurement errors (see Fig. 2). This leads to the following errors-in- variables stochastic framework

$$\begin{aligned} Y(k) &= Y_0(k) + N_Y(k) \\ U(k) &= U_0(k) + N_U(k) \end{aligned} \quad (14)$$

with $Y(k)$, $U(k)$ the scaled input/output DFT spectra (2), $Y_0(k) = G_R(s_k)U_0(k)$, $U_0(k)$ the true (unknown) values, and $N_Y(k) = M_Y(k) + Y_S(k)$, $N_U(k) = M_U(k)$ the additive errors. Equation (14) can be summarized as $Z(k) = Z_0(k) + N_Z(k)$ with $Z^T(k) = [Y(k)U(k)]$ and similarly for $Z_0(k)$ and $N_Z(k)$. The related linear dynamic system $G_R(s_k)$ is modeled by a rational transfer function in the Laplace variable s

$$G(s, \theta) = \frac{B(s, \theta)}{A(s, \theta)} = \frac{\sum_{r=0}^{n_b} b_r s^r}{\sum_{r=0}^{n_a} a_r s^r} \quad (15)$$

where $\theta^T = [a_0 a_1 \cdots a_{n_a} b_0 b_1 \cdots b_{n_b}]$ is the vector of the model parameters, and $A(s, \theta)$, $B(s, \theta)$ are, respectively, the denominator and numerator polynomials. Since $G(s, \lambda\theta) = G(s, \theta)$ for $\lambda \neq 0$, there is a parameter ambiguity in (15) and, therefore, the model parameters must be constrained, for example, $a_i = 1$, $b_j = 1$ or $||\theta||_2^2 = 1$.

B. Maximum Likelihood Estimator

Following the lines of [3], [9] the maximum likelihood (ML) estimator $\hat{\theta}_{\mathrm{ML}}(Z)$ can be constructed. Its cost function is given by

$$V_{\mathrm{ML}}(\theta, Z) = \sum_{k=1}^{F} \frac{|e(s_k, \theta, Z(k))|^2}{\sigma_e^2(s_k, \theta)} \quad (16)$$

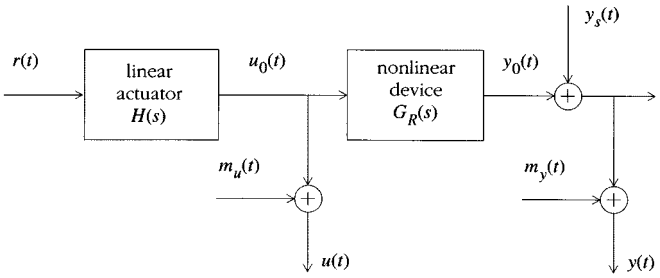

Fig. 2. Measurement of the best linear approximation $G_R(s)$ of a nonlinear device: $u_0(t)$, $y_0(t)$ are the true input/output signals; $m_u(t)$, $m_y(t)$ are the input/output measurement errors; $y_s(t)$ is the zero mean stochastic nonlinear contribution; $r(t)$ is the reference signal (typically the waveform stored in the arbitrary waveform generator).

with $Z^T = [Z^T(1)Z^2(2)\cdots Z^T(N)]$ and

$$e(s_k, \theta, Z(k)) = A(s_k, \theta)Y(k) - B(s_k, \theta)U(k) \quad (17)$$

$$\begin{aligned} \sigma_e^2(s_k, \theta) = {} & |A(s_k, \theta)|^2\sigma_Y^2(k) + |B(s_k, \theta)|^2\sigma_U^2(k) \\ & - 2\mathrm{Re}\left(A(s_k, \theta)\overline{B}(s_k, \theta)\sigma_{YU}^2(k)\right) \end{aligned} \quad (18)$$

$$\sigma_Y^2 = \mathrm{var}(N_Y(k)), \qquad \sigma_U^2(k) = \mathrm{var}(N_U(k)),$$

and

$$\sigma_{YU}^2(k) = \mathrm{covar}(N_Y(k), N_U(k)). \quad (19)$$

$e(s_k, \theta, Z(k))$ is the equation error of the model and $\sigma_e^2(s_k, \theta) = \mathrm{var}(e(s_k, \theta, N_Z(k)))$ the variance of the equation error where the measurements are replaced by the noise on the measurements. The ML estimate (16) of the related linear dynamic system has exactly the same properties of the ML estimate of a linear dynamic system [9] (proof: see Appendix I). Note that the ML estimator (16) requires the knowledge of the noise (co-)variances.

C. Measurement Strategy

An estimate of the noise (co-)variances (19) is obtained through the following measurement strategy:

1) Choose the amplitude spectrum $|A(kf_s/N)|$ of the random-phase multisine (see Definition 1).
2) Make a random choice of the phases $\angle A(kf_s/N)$, $k = 1, 2, \ldots, F$ of the random-phase multisine (see Definition 1) and calculate the corresponding time signal $r(t)$.
3) Apply the excitation to the device under test and measure $P \geq 1$ periods of the steady state response $u(t)$, $y(t)$.
4) Repeat steps 2. and 3. $M \geq 6$ times.[1]

[1] $M = 6$ is the minimal number of experiments required to preserve the asymptotic $(N \to \infty)$ properties of the maximum likelihood estimator (16) (see [12]).

5) Calculate the DFT spectra of the input $u(t)$, output $y(t)$, and reference $r(t)$ signals for each experiment at the excited DFT frequencies. This gives M sets of the reference $R^{[m]}(k)$, noisy input $U^{[m]}(k)$, and noisy output $Y^{[m]}(k)$ spectra, $k = 1, 2, \ldots, F$ and $m = 1, 2, \ldots, M$.
6) Project the input and output spectra on the reference spectrum

$$Y_R^{[m]}(k) = Y^{[m]}(k)/R^{[m]}(k),$$
$$U_R^{[m]}(k) = U^{[m]}(k)/R^{[m]}(k) \tag{20}$$

and finally calculate the sample mean and sample (co-)variances

$$\hat{Y}(k) = \frac{1}{M}\sum_{m=1}^{M} Y_R^{[m]}(k),$$
$$\hat{U}(k) = \frac{1}{M}\sum_{m=1}^{M} U_R^{[m]}(k) \tag{21}$$
$$\hat{\sigma}_Y^2(k) = \frac{1}{M-1}\sum_{m=1}^{M}\left|\hat{Y}(k) - Y_R^{[m]}(k)\right|^2$$
$$\hat{\sigma}_U^2(k) = \frac{1}{M-1}\sum_{m=1}^{M}\left|\hat{U}(k) - U_R^{[m]}(k)\right|^2$$
$$\hat{\sigma}_{YU}^2(k) = \frac{1}{m-1}\sum_{m=1}^{M}\left(\hat{Y}(k) - Y_R^{[m]}(k)\right)\overline{\left(\hat{U}(k) - U_R^{[m]}(k)\right)}. \tag{22}$$

Notes

- The stochastic nonlinear contribution $y_s(t)$ (Fig. 2) is a periodic signal, which has the same periodicity as the corresponding reference signal $r(t)$. Calculating the sample (co-)variances over one experiment [one realization of the phases $\angle A(kf_s/N)$] will hence only give information about the measurement errors $M_Y(k)$ and $M_U(k)$ in (14), but not about the stochastic nonlinear contributions $Y_S(k)$. Different realizations of the phases $\angle A(kf_s/N$ are required to get the contribution of $Y_S(k)$ into the sample (co-)variances.
- Due to the random choice of the phase $\angle A(kf_s/N)$ over the different realizations of the reference signal $r(t)$, the phases of the true input/output spectra will be scattered in the interval $[0, 2\pi)$. Therefore, in step 6. of the measurement strategy, the input/output spectra must be projected on the reference spectrum; otherwise, the sample means would tend to zero as M increases to infinity (see Appendix II).
- It is well known that (12) will introduce a (small) bias when the input $U(k)$ is disturbed by measurement noise [10]. This means that the estimate

$$\hat{G}_R(s_k) = \frac{1}{M}\sum_{m=1}^{M}\frac{Y^{[m]}(k)}{U^{[m]}(k)} \tag{23}$$

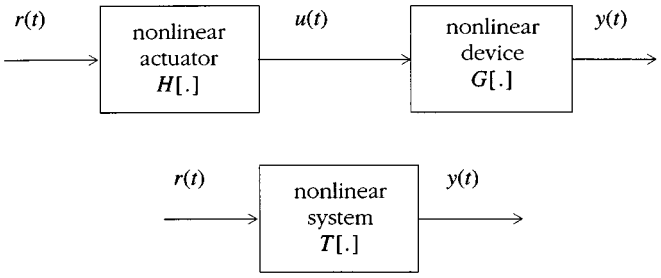

Fig. 3. Schematic representation of a nonlinear device loading the generator nonlinearly: the input $u(t)$ of the device is nonlinearly related to the reference signal $r(t)$. The overall system from the reference $r(t)$ to the output of the device is denoted by $T[.]$.

will not converge to the true value $G_R(s_k)$ as M increases to infinity. The bias can be avoided by taking the ratio of the sample means (21)

$$\hat{G}_R(s_k) = \frac{\hat{Y}(k)}{\hat{U}(k)} = \frac{\frac{1}{M}\sum_{m=1}^{M} Y_R^{[m]}(k)}{\frac{1}{M}\sum_{m=1}^{M} U_R^{[m]}(k)}. \tag{24}$$

Indeed, using the strong law of large numbers [11], it follows that (24) converges strongly ($M \to \infty$) to $E\{Y_R(k)\}/E\{U_R(k)\}$, which is exactly $G_R(s_k)$ (see Appendix II).

- It may happen that the nonlinear device loads the generator nonlinearly or that the actuator itself is nonlinear, creating nonlinear distortions at the input. Fig. 3 shows the corresponding block diagram. Applying the measurement strategy to this situation gives an estimate $\hat{G}_R(s_k) = \hat{Y}(k)/\hat{U}(k)$ which converges strongly to $E\{Y_R(k)\}/E\{U_R(k)\} = T_R(s_k)/H_R(s_k)$, where $T_R(s_k)$ and $H_R(s_k)$ are the related linear dynamic systems of the nonlinear systems $T[\cdot]$ and $H[\cdot]$, respectively (see Appendix III). Note that in general $T_R(s_k)/H_R(s_k) \neq G_R(s_k)$; however, if the nonlinear distortions at the input are small, $\text{var}(U_S(k)) \ll |H_R(s_k)R(k)|^2$, or if the best linear approximation of the device $G_R(s_k)$ is not very sensitive to (small) variations of the input power spectrum, then $T_R(s_k)/H_R(s_k) \approx G_R(s_k)$.

D. Estimator Based on the Sample Mean and Sample (Co-)Variances

Putting the sample mean (21) and sample variances (22) in the ML cost function (16) defines a new estimator

$$V_{\text{SML}}(\theta, Z) = \sum_{k=1}^{N}\frac{\left|\hat{\varepsilon}\left(s_k, \theta, \hat{Z}(k)\right)\right|^2}{\hat{\sigma}_{\hat{\varepsilon}}^2(s_k, \theta)} \tag{25}$$

with

$$\hat{e}\left(s_k, \theta, \hat{Z}(k)\right) = A(s_k, \theta)\hat{Y}(k) - B(s_k, \theta)\hat{U}(k) \tag{26}$$

$$\hat{\sigma}^2_{\hat{e}}(s_k, \theta) = |A(s_k, \theta)|^2\hat{\sigma}^2_{\hat{Y}}(k) + |B(s_k, \theta)|^2\hat{\sigma}^2_{\hat{U}}(k) - 2\mathrm{Re}\left(A(s_k, \theta)\overline{B}(s_k, \theta)\hat{\sigma}^2_{\hat{Y}\hat{U}}(k)\right) \tag{27}$$

$$\hat{\sigma}^2_{\hat{Y}}(k) = \hat{\sigma}^2_{Y}(k)/M, \qquad \hat{\sigma}^2_{\hat{U}}(k) = \hat{\sigma}^2_{U}(k)/M,$$

and

$$\hat{\sigma}^2_{\hat{Y}\hat{U}}(k) = \hat{\sigma}^2_{YU}(k)/M. \tag{28}$$

The minimizer $\hat{\theta}_{\mathrm{SML}}(Z)$ of (25) has exactly the same asymptotic ($N \to \infty$) properties as in [12]; for example, if the model order n_b over n_a is sufficiently high, then the estimated transfer function model $G(s, \hat{\theta}_{\mathrm{SML}}(Z))$ converges strongly to the related linear dynamic system $G_R(s_k)$ (proof: see Appendix IV).

IV. Simulation Example

As a simulation example we take a Wiener–Hammerstein system (see Fig. 4) with

$$G_1(s) = \frac{1}{s^2/\omega_0^2 + s/(Q\omega_0) + 1}, \qquad f = \tanh,$$

and

$$G_2(s) = \frac{1}{s/\omega_{3\ \mathrm{dB}} + 1} \tag{29}$$

(see Table I for the values of f_0, Q, and $f_{3\ \mathrm{dB}}$). The input signal $u(t)$ is a random-phase multisine (1) with $f_s = 50$ kHz, $f_{\max} = 2$ kHz, $N = 12\,500$, $|A(kf_s/N| = \sqrt{N/(2F)}$, and $F = Nf_{\max}/f_s$ the number of sinewaves. For this choice of the parameters, $u(t)$ contains $F = 500$ sinewaves and has an rms value of 1. N input/output samples of the steady state response are calculated at the sampling rate f_s. In [1], it has been shown that the best linear approximation of the Wiener–Hammerstein system equals

$$G_R(s) = KG_1(s)G_2(s) \tag{30}$$

for N, and hence also F, sufficiently large. K depends on the static nonlinearity and the power spectrum of the excitation signal, but is independent of the frequency. Since (30) is only asymptotically ($F \to \infty$) valid, the errors-in-variables approach of Section III is validated by comparing the estimates with the case where no measurement noise is present [$M_U(k) = 0, M_Y(k) = 0$]. Therefore, two data sets are generated: one with and one without measurement noise. In the data set with measurement noise, the noiseless $u_0(t)$ input $y_0(t)$ output signals are disturbed by white Gaussian noise with zero mean and standard deviation $\sqrt{N/(2F)} = 3.5$ and $0.15\sqrt{N/(2F)} = 0.53$, respectively. Note that the input measurement noise is 3.5 times larger that the noiseless input signal.

The corresponding signal-to-noise ratios (SNRs) per spectral line of one period of the steady state response are shown in Fig. 5. It follows that the input SNR per spectral line is 1 (0 dB). The output SNR of the simulation without measurement noise is a measure of the variance of the stochastic nonlinear contribution $Y_S(k)$ in (5). The measurement strategy of Section III-C is applied with $r(t) = u_0(t)$, $P = 1$, and $M = 4$. This increases the SNRs of the data with a factor of 2 (6 dB). One thousand data sets (21) and (22) are generated for the case with and the case without measurement noise.

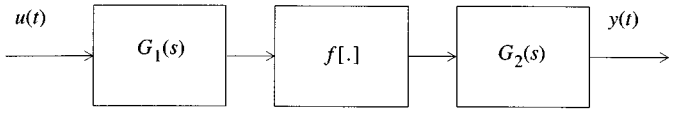

Fig. 4. Wiener–Hammerstein system consisting of the cascade of a linear dynamic block $G_1(s)$, a static nonlinear block $f[.]$, and a linear dynamic block $G_2(s)$.

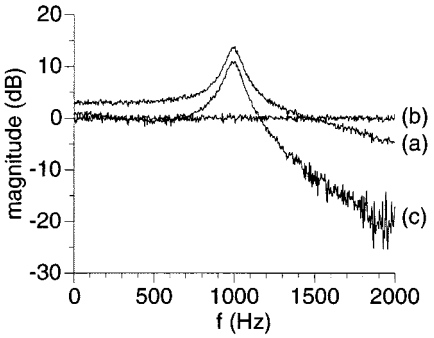

Fig. 5. Signal-to-noise ratios (SNRs) of the simulations calculated using the measurement strategy of Section III-C with $r(t) = u_0(t)$, $P = 1$ and $M = 400$: (a) output SNR of the simulation without measurement noise; (b) and (c), respectively, the input and output SNR of the simulation with measurement noise.

Fig. 6 shows the frequency response function (24) of one such data set. A transfer function model (15) with $n_a = 3$ and $n_b = 0$ is estimated for each data set. The results are shown in Fig. 7 and Table I. From Fig. 7, it follows that the estimated transfer function models for the case with and the case without measurement noise coincide. From Table I, it follows that the estimated model parameters in the case without measurement noise are quite close but not equal to their asymptotic values. This is due to the finite value of F (and N). Increasing F (and N) makes the differences decrease to zero as $O(F^{-1})$ as predicted by the theory [1]. The estimated model parameters, except the Q-factor, for the cases with and without measurement noise coincide.

V. Real Measurement Example

The device under test (DUT) is a Wiener–Hammerstein system (Fig. 4) consisting of the cascade of a third order Chebyshev filter (passband ripple of 0.5 dB and cut off frequency of 4.4 kHz), a static nonlinear system (see Fig. 8), and a third order inverse Chebyshev filter (stopband attenuation of 40 dB starting at 5 kHz). The input and output of the active filters are voltage buffered. Asymptotically [the number of frequencies in the random-phase multisine (1) goes to infinity], the best linear approximation of the nonlinear system is given by

$$G_R(s) = KG_0(s) \quad \text{with} \quad G_0(s) = \frac{b_0 + b_1 s + b_2 s^2}{a_0 + a_1 s + \cdots + a_6 s^6} \tag{31}$$

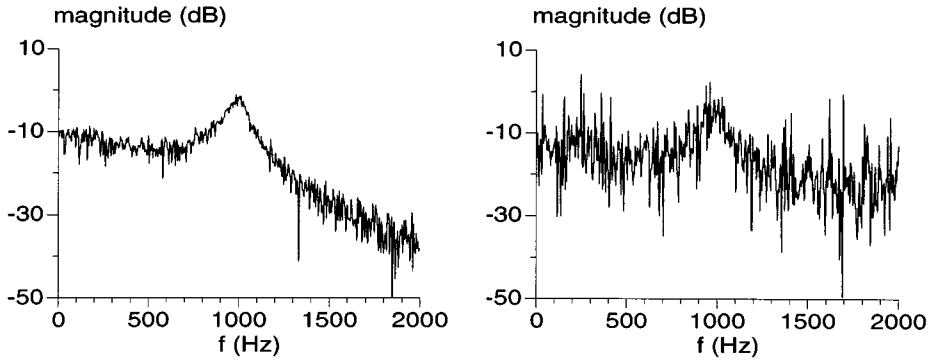

(a) (b)

Fig. 6. Frequency response function $\hat{G}_R(s_k)$ (24), calculated using $M = 4$ independent repeated experiments. (a) Without measurement noise, (b) with measurement noise.

TABLE I
RESULT OF THE MONTE-CARLO SIMULATION (1000 RUNS). MEAN VALUE OF THE ESTIMATED MODEL PARAMETERS WITH AND WITHOUT MEASUREMENT NOISE TOGETHER WITH THEIR 95% CONFIDENCE BOUND

	asymptotic value ($N \to \infty$)	estimate without measurement noise	estimate with measurement noise
f_0 (Hz)	1000	999.930 ± 0.070	1000.27 ± 0.32
Q	10	10.033 ± 0.019	10.155 ± 0.070
f_{3dB} (Hz)	300	300.94 ± 0.70	301.7 ± 2.0
K	-	0.27068 ± 0.00056	0.2721 ± 0.0015

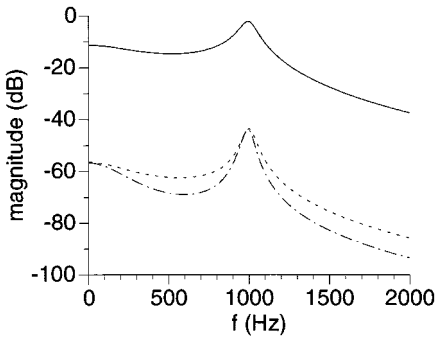

Fig. 7. Result of the Monte-Carlo simulation (1000 runs). Mean value of the estimated transfer function models with and without measurement noise (solid line), difference between the mean values (dash-dot line), and 95% confidence bound of the mean value with measurement noise (dashed line).

where K is a frequency-independent constant depending on the static nonlinear system and the power spectrum of the input signal, and $G_0(s)$ is the cascade of the two linear parts.

The DUT is measured using random-phase multisines (1) with $F = 500$, $f_{\max} = 10$ kHz, $f_s = 20$ MHz/64 ($N = 15\,625$), and $|A(kf_s/N)| = c$, $k = 1, 2, \ldots, F$ with c independent of k. The signals are generated (HP model E1445A) and measured (HP model E1437A) at the sampling frequency f_s, which is derived from a common 20 MHz mother clock. Following the strategy of Section III-C with $M = P = 16$, the small (rms value of 25 mV) and large (rms value of 400 mV) signal response of the DUT are measured.

Fig. 9(a) shows the corresponding frequency response functions (FRFs) calculated using (24). Note that the large signal FRF $\hat{G}_R(s_k)$ is much "noisier" than the small signal FRF $\hat{G}_0(s_k)$. This is entirely due to the stochastic nonlinear contributions $Y_S(k)$ and not to the measurement errors $M_U(k)$ and $M_Y(k)$. Fig. 9(a) suggests that both FRFs are equal within a frequency-independent gain factor. To verify this, the residual

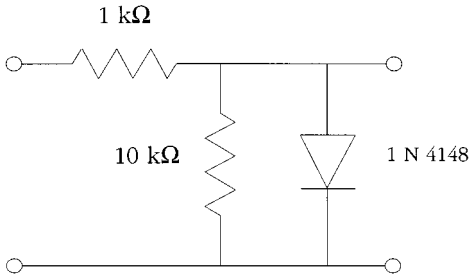

Fig. 8. Static nonlinear system consisting of two resistors and one diode.

$$\hat{G}_R(s_k) - \hat{K}\hat{G}_0(s_k) \tag{32}$$

is calculated, where $\hat{K}$ is the mean gain between both FRFs in the passband of the DUT,

$$\hat{K} = \frac{1}{R}\sum_{k=1}^{R} |\hat{G}_R(s_k)/\hat{G}_0(s_k)| \quad \text{with} \quad R = 200. \tag{33}$$

Fig. 9(b) shows the residual (32) and its 95% uncertainty bound. It follows that $\hat{G}_R(s_k) = \hat{K}\hat{G}_0(s_k)$ within the measurement uncertainty, which experimentally confirms (31). Using the large signal measurements (400 mV rms), the sample maximum likelihood (SML) estimate $\hat{\theta}_{\mathrm{SML}}(Z)$ (25) of transfer function model (31) is calculated. In the absence of model errors, the 95% confidence interval of the minimum of the cost function equals

$$\left(F - \frac{n_\theta}{2}\right)\frac{M-1}{M-2} \pm 2\sqrt{\frac{(M-1)^3}{(M-2)^2(M-3)}\,F} \approx 530.9 \pm 25.7 \tag{34}$$

(see [12]). Comparing (34) to the actual value $V_{\mathrm{SML}}(\hat{\theta}_{\mathrm{SML}}(Z), Z) = 557.3$, it can be concluded that almost no model errors can be detected [14]. Fig. 10 shows

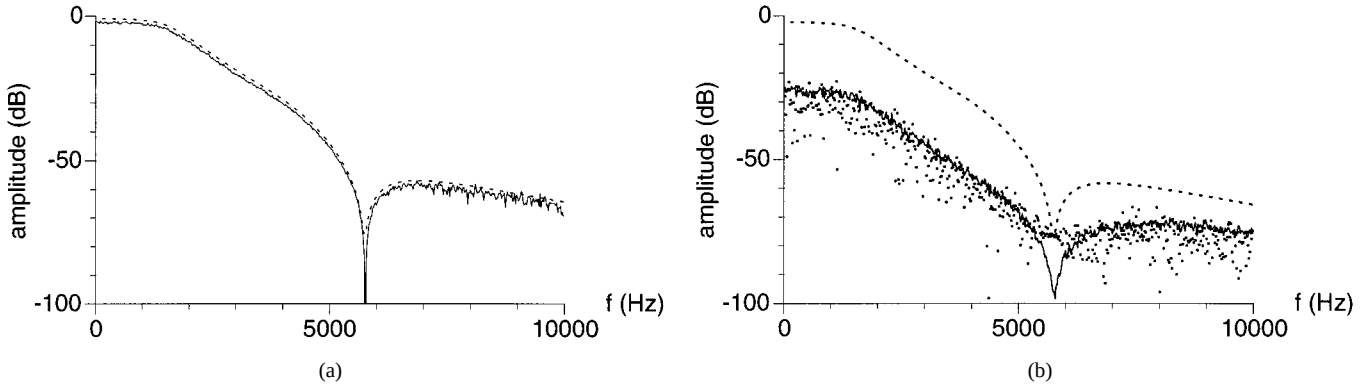

Fig. 9. Frequency response function (FRF) measurement of the Wiener–Hammerstein system. (a) Comparison between the small signal FRF $\hat{G}_0(s_k)$ (dashed line) and the large signal FRF $\hat{G}_R(s_k)$ (solid line). (b) The residual $\hat{G}_R(s_k) - \hat{K}\hat{G}_0(s_k)$ (32) (dots), its 95% uncertainty bound (bold line), and the FRF $\hat{K}\hat{G}_0(s_k)$ (dashed line).

the difference between the identified large signal model $G(s_k, \hat{\theta}_{\mathrm{SML}}(Z))$ and the small signal FRF $\hat{G}_0(s_k)$

$$G(s_k, \hat{\theta}_{\mathrm{SML}}(Z)) - \hat{K}\hat{G}_0(s_k) \tag{35}$$

where $\hat{K}$ is calculated as

$$\hat{K} = \frac{1}{R}\sum_{k=1}^{R} |G(s_k, \hat{\theta}_{\mathrm{SML}}(Z))/\hat{G}_0(s_k)| \quad \text{with} \quad R = 200. \tag{36}$$

It can be concluded that $G(s_k, \hat{\theta}_{\mathrm{SML}}(Z)) = \hat{K}\hat{G}_0(s_k)$ from dc to 4 kHz. This is approximately true in the band 6 kHz to 10 kHz (the residuals are larger than their uncertainty). This is confirmed by modeling the small signal (25 mV rms) experiment, where it turns out that a rational transfer function of order 6/6 is needed to explain the measurements (the two additional zeros in this model lie outside the 10 kHz band).

Two additional measurements have been performed: one with a Schroeder phase multisine [(1) with $\angle A(kf_s/N) = -\pi k(k-1)/F$], and one with periodic Gaussian noise [eq. (1) with circular complex Gaussian distributed $A(kf_s/N)$]. Both signals have the same power spectrum (and rms value) as the large signal random-phase multisines of the previous experiments (rms value of 400 mV). Fig. 11 compares the Schroeder FRF with the large (400 mV rms) and small (25 mV rms) signal FRFs obtained with the random-phase multisines (measurement strategy of Section III-C with $P = 16$ and $M = 1$). Clearly, the behavior of the Schroeder multisine is completely different from the random-phase multisines: the Schroeder FRF is smooth and wrongly suggests the presence of a large number of poles in the passband of the DUT, while the large signal (random-phase multisine) FRF is rather noisy. It clearly illustrates that the theory presented in this paper is valid, only if the phases of the excitation signal are random.

To illustrate the power (and limitation) of the best linear approximation of a nonlinear device, the response $y(t)$ of one period of the periodic noise experiment has been predicted using the previously identified model $G(s, \hat{\theta}_{\mathrm{SML}}(Z))$. The prediction $\hat{y}(t)$ is calculated as

$$\hat{y}(t) = \mathrm{IDFT}(G(s_k, \hat{\theta}_{\mathrm{SML}}(Z))U(k)) \tag{37}$$

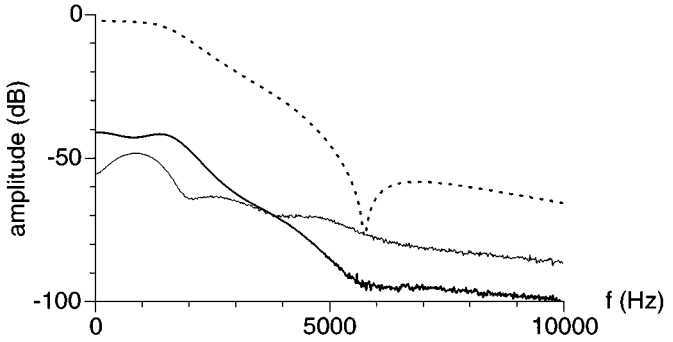

Fig. 10. Comparison between the small signal FRF $\hat{G}_0(s_k)$ and the modeled large signal FRF $G_R(s_k, \hat{\theta}_{\mathrm{SML}}(Z))$: the residual $G_R(s_k, \hat{\theta}_{\mathrm{SML}}(Z)) - \hat{K}\hat{G}_0(s_k)$ (35) (solid line), its 95% uncertainty bound (bold line), and the FRF $\hat{K}\hat{G}_0(s_k)$ (dashed line).

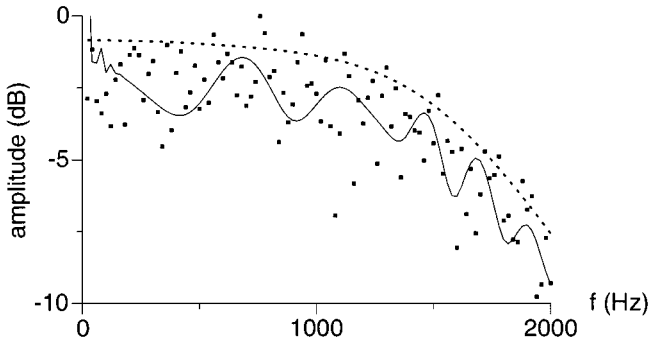

Fig. 11. Frequency response function (FRF) measurement of the passband of the Wiener–Hammerstein system using: (a) a small signal (25 mV rms) random-phase multisine (dashed line), (b) a large signal (400 mV rms) random-phase multisine (dots), and (c) a large signal (400 mV rms) Schroeder phase multisine (solid line). For each experiment the measurement strategy of Section III-C is followed with $P = 16$ and $M = 1$.

with $U(k)$ the measured input DFT spectrum of the periodic noise experiment and IDFT the inverse discrete Fourier transform. Fig. 12 compares the predicted output $\hat{y}(t)$ to the measured output $y(t)$. It can be seen that the prediction error $\hat{y}(t) - y(t)$ is about ten times smaller than $y(t)$. This error is entirely due to the stochastic nonlinear distortions $y_s(t) = \mathrm{IDFT}(Y_S(k))$ and not to the measurement errors $m_u(t)$ and $m_y(t)$. Therefore, using a linear model, it is impossible to reduce the prediction error below the level of the

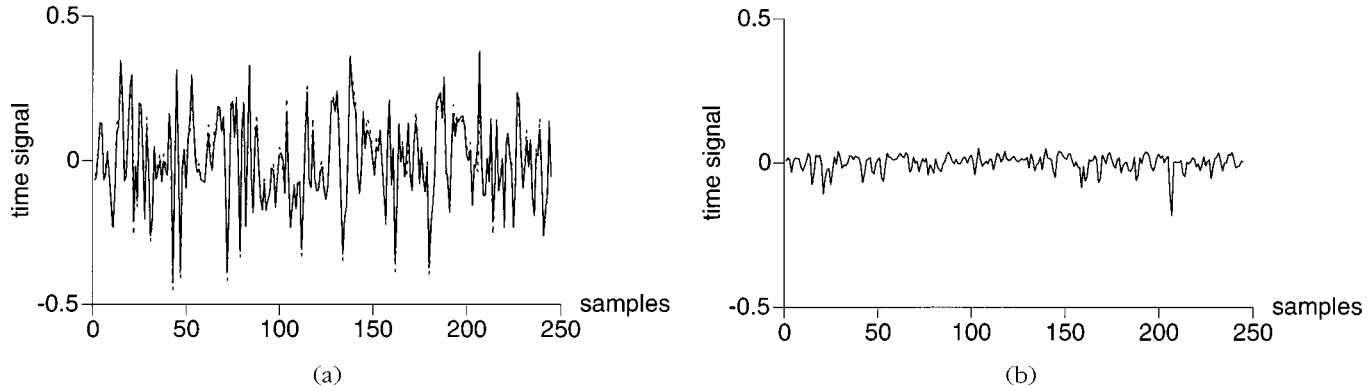

Fig. 12. Prediction of one period of the steady state response of the Wiener–Hammerstein system to a periodic Gaussian noise excitation (400 mV rms) with the same power spectrum as the large signal (400 mV rms) random-phase multisines. (a) Predicted output $\hat{y}(t)$ (solid line) and measured output $y(t)$ (dashed line). (b) Difference $\hat{y}(t) - y(t)$.

stochastic nonlinear contributions $y_s(t)$. Note that the 10% error level in Fig. 12(b) corresponds to the 1 dB fluctuations (rms value) of the FRF measurement with the large signal random-phase multisine in Fig. 11. Note also that, although $\hat{y}(t) - y(t)$ in Fig. 12(b) has a random-like behavior, it is a periodic signal with the same periodicity as $y(t)$.

VI. Conclusion

In this paper, the identification of linear systems in the presence of nonlinear distortions is discussed. A related linear dynamic system (best linear approximation) of the overall system is introduced, which is valid for a general class of excitation signals, and a general class of (strongly) nonlinear systems. This best linear approximation can be identified using a general measurement setup where both the input and output are disturbed by measurement errors. Using the best linear approximation, the response of the nonlinear system can be predicted within an error that is bounded below by the stochastic nonlinear contributions.

Appendix I

Multiplying the errors-in-variables model (14) by $e^{-j\angle U_0(k)}$ gives

$$\begin{aligned} Y(k)e^{-j\angle U_0(k)} &= G_R(s_k)|U_0(k)| + N_Y(k)e^{-j\angle U_0(k)} \\ U(k)e^{-j\angle U_0(k)} &= |U_0(k)| + N_U(k)e^{-j\angle U_0(k)}. \end{aligned} \tag{38}$$

Note that this phase shift does not change the cost function (16). The noisy part $N_Z(k)e^{-j\angle U_0(k)}$ of (38) is independent of the signal part $|U_0(k)|$. In [1], it has been shown that $Y_S(k)/U_0(k)$ has the same stochastic properties as the measurement errors $M_U(k)$ and $M_Y(k)$. Since the phase of $Y_S(k)e^{-j\angle U_0(k)}$ equals the phase of $Y_S(k)/U_0(k)$, this is also valid for $Y_S(k)e^{-j\angle U_0(k)}$. We conclude that $N_Z(k)e^{-j\angle U_0(k)}$ has the same properties as the measurement errors. The only difference with the identification of a linear dynamic system $G_0(s)$ is that the linear dynamic system is replaced by the related linear dynamic system $G_R(s)$.

Appendix II

Relating the true input and output spectra in (14) to the reference spectrum gives

$$\begin{aligned} Y(k) &= G_R(s_k)H(s_k)R(k) + N_Y(k) \\ U(k) &= H(s_k)R(k) + N_U(k). \end{aligned} \tag{39}$$

Taking the expected value of (39) w.r.t. the measurement noise and the random-phase $\angle A(kf_s/N)$ of $R(k)$ shows that $E\{Y(k)\} = 0$ and $E\{U(k)\} = 0$. Dividing both sides of (39) by $R(k)$ gives

$$\begin{aligned} Y_R(k) &= G_R(s_k)H(s_k) + N_{Y_R}(k) \\ U_R(k) &= H(s_k) + N_{U_R}(k) \end{aligned} \tag{40}$$

with $X_R(k) = X(k)/R(k)$, and $N_{X_R}(k) = N_X(k)/R(k)$, $X = Y$ and U. Note that the noise (co-)variances of $N_{Y_R}(k)$ and $N_{U_R}(k)$ equal those of $N_Y(k)$ and $N_U(k)$ divided by $|R(k)|^2$. Taking the expected value of (40) w.r.t. the measurement noise and the random-phase $\angle A(kf_s/N)$ of $R(k)$ gives $E\{Y_R(k)\}/E\{U_R(k)\} = G_R(s_k)$.

Appendix III

Applying (5) to the nonlinear operators $T[.]$ and $H[.]$ gives, taking into account the measurement errors $M_U(k)$, $M_Y(k)$,

$$\begin{aligned} Y(k) &= T_R(s_k)R(k) + N_Y(k) \\ U(k) &= H_R(s_k)R(k) + N_U(k) \end{aligned} \tag{41}$$

with $N_Y(k) = Y_S(k) + M_Y(k)$, $N_U(k) = U_S(k) + M_U(k)$, and $Y_S(k)$, $U_S(k)$ the zero mean nonlinear distortions which are uncorrelated with the reference $R(k)$. Dividing both sides of (41) by $R(k)$ and taking the expected value w.r.t. to the measurement noise and the random-phase $\angle A(kf_s/N)$ of $R(k)$ shows that $E\{Y_R(k)\}/E\{U_R(k)\} = T_R(s_k)/H_R(s_k)$, where $Y_R(k)$, $U_R(k)$ are defined as in Appendix II.

APPENDIX IV

In [12], the properties of the SML estimator for linear dynamic systems has been studied assuming that the frequency domain errors are independent (over the frequency) and normally distributed. It makes sense to study the properties of (25) under these idealized assumptions if they are met asymptotically ($F \to \infty$). First note that the noise $N_Z(k)e^{-j\angle U_0(k)}$ has the same stochastic properties as the measurement noise $M_U(k)$ and $M_Y(k)$ (see Appendix I). Next, it is sufficient to prove that $Y_S(k)e^{-j\angle U_0(k)}$ is asymptotically normally distributed. From [1], it follows that $Y_S(k)$ consists of the sum of $O(F)$ independent random variables with bounded moments of order three. Hence, $Y_S(k)$ is asymptotically normally distributed at the rate $O(F^{-1/2})$ (proof: see [13, Th. 9.1.3]).

REFERENCES

[1] J. Schoukens, T. Dobrowiecki, and R. Pintelon, "Parametric identification of linear systems in the presence of nonlinear distortions. A frequency domain approach," *IEEE Trans. Automat. Contr.*, vol. 43, pp. 176–190, Feb. 1998.

[2] L. Ljung, *System Identification: Theory for the User*. Upper Saddle River, NJ: Prentice–Hall, 1999.

[3] J. Schoukens and R. Pintelon, *Identification of Linear Systems: A Practical Guideline to Accurate Modeling*. London, U.K.: Pergamon, 1991.

[4] J. Schoukens, J. Swevers, J. De Cuyper, and Y. Rolain, "Simple methods and insights to deal with nonlinear distortions in FRF-measurements," in *Proc. ISMA23 Int. Conf. Noise Vibration Eng.*, Leuven, Belgium, Sept. 16–18, 1998, pp. 337–342.

[5] C. Evans and D. Rees, "Nonlinear distortions and multisine signals. Part I: Measuring the best linear approximation," *IEEE Trans. Instrum. Meas.*, vol. 49, pp. 602–609, June 2000.

[6] C. Evans and D. Rees, "Nonlinear distortions and multisine signals. Part II: Minimizing the distortion," *IEEE Trans. Instrum. Meas.*, vol. 49, pp. 610–616, June 2000.

[7] M. Schetzen, *The Volterra and Wiener Theories of Nonlinear Systems*. New York: Wiley, 1980.

[8] L. O. Chua and C.-Y. Ng, "Frequency domain analysis of nonlinear systems: General theory," *Electron. Circuits Syst.*, vol. 3, no. 4, pp. 165–185, 1979.

[9] R. Pintelon, P. Guillaume, Y. Rolain, J. Schoukens, and H. Van hamme, "Parametric identification of transfer functions in the frequency domain, a survey," *IEEE Trans. Automat. Contr.*, vol. 39, pp. 2245–2260, Nov. 1994.

[10] P. Guillaume, P. Pintelon, and J. Schoukens, "Nonparametric frequency response functions estimators based on nonlinear averaging techniques," *IEEE Trans. Instrum. Meas.*, vol. 41, pp. 739–746, Dec. 1992.

[11] E. Lukacs, *Stochastic Convergence*. New York: Academic, 1975.

[12] J. Schoukens, G. Vandersteen, R. Pintelon, and P. Guillaume, "Frequency domain system identification using nonparametric noise models estimated from a small number of data sets," *Automatica*, vol. 33, no. 6, pp. 1073–1086, 1997.

[13] Y. S. Chow and H. Teicher, *Probability Theory: Independence, Interchangeability, Martingales*, 2nd ed. New York: Springer-Verlag, 1988.

[14] R. Pintelon, J. Schoukens, and G. Vandersteen, "Model selection through a statistical analysis of the global minimum of a weighted nonlinear least squares cost function," *IEEE Trans. Signal Processing*, vol. 45, pp. 686–693, Mar. 1997.

Rik Pintelon (M'90–SM'96–F'98) was born in Gent, Belgium, on December 4, 1959. He received the Electrotechnical-Mechanical Engineer (burgerlijk ingenieur) degree in July 1982, the Doctor in applied sciences degree in January 1988, and the qualification to teach at university level (geaggregeerde voor het hoger onderwijs) in April 1994, all from the Vrije Universiteit Brussel (VUB), Brussels, Belgium.

He is presently a Professor in the Electrical Measurement Department (ELEC), VUB. His main research interests are in the field of parameter estimation/system identification, and signal processing.

Johan Schoukens (M'90–SM'92–F'97) was born in Belgium in 1957. He received the Engineer degree in 1980 and the Doctor degree in applied sciences in 1985, both from the Vrije Universiteit Brussel (VUB), Brussels, Belgium.

He is presently a Professor at the VUB. The prime factors of his interest are in the field of system identification for linear and nonlinear systems, and growing tomatoes in his green house.

Wendy Van Moer (S'98) received the Electrotechnical Engineer degree (telecommunication) in 1997 from the Vrije Universiteit Brussel (VUB), Brussels, Belgium.

She is presently a Researcher of the IWT in the Electrical Measurement Department (ELEC), VUB. Her main research interests are nonlinear microwave measurement and modeling techniques.

Yves Rolain (M'90–SM'96) is presently active in the Electrical Measurement Department (ELEC), Vrije Universiteit Brussel, Brussels, Belgium . His main research interests are nonlinear microwave measurement techniques, applied digital signal processing, parameter estimation/system identification, and biological agriculture.